First-principles elastic constants for the hcp transition metals Fe, Co, and Re at high pressure

Gerd Steinle-Neumann and Lars Stixrude
Department of Geological Sciences, University of Michigan, Ann Arbor, Michigan 48109-1063

Ronald E. Cohen
Geophysical Laboratory and Center for High Pressure Research, Washington, DC 20015-1305
(Received 8 September 1998; revised manuscript received 16 February 1999)

The elastic constant tensors for the hcp phases of three transition metals (Co, Re, and Fe) are computed as functions of pressure using the linearized augmented plane wave method with both the local density and generalized gradient approximations. Spin-polarized states are found to be stable for Co (ferromagnetic) and Fe (antiferromagnetic at low pressure). The elastic constants of Co and Re are compared to experimental measurements near ambient conditions and excellent agreement is found. Recent measurements of the lattice strain in high pressure experiments when interpreted in terms of elastic constants for Re and Fe are inconsistent with the calculated moduli. [S0163-1829(99)13525-2]

I. INTRODUCTION

The effect of pressure on the propagation of elastic waves in materials is essential for understanding interatomic interactions, mechanical stability of solids, phase transition mechanisms, material strength, and the internal structure of Earth and other planets. However, little is known of the elasticity of solids at high pressure. The experimental study of the elasticity of materials under high pressure is challenging, as traditional methods have been applied only to moderate pressures. Ultrasonic measurements are generally limited to a few GPa,[1] while Brillouin spectroscopy has been applied up to 25 GPa.[2]

We investigate the elasticity of three hexagonal transition metals at high pressure: iron, rhenium, and cobalt. High pressure properties of iron are of considerable geophysical interest as Earth's solid inner core is composed primarily of this element. The elasticity of hcp iron is important for understanding the elastic anisotropy of the inner core,[3–5] and its super-rotation.[6] Rhenium is the strongest metal known at high pressure[7] and is widely used as a gasket material in diamond anvil cell experiments. We have chosen cobalt for this study because of its proximity to iron in the periodic table and as an example of a ferromagnetic hcp metal.

All three of these metals have been studied experimentally under high pressure and their equations of state are well known. Iron transforms from the bcc phase at ambient conditions to hcp near 13 GPa;[8] the equation of state of the hcp phase has been measured up to 300 GPa.[9] Recent advances in diamond anvil cell techniques have made it possible to evaluate the lattice strain in a polycrystal subjected to a nonhydrostatic stress field which can be associated with elastic constants. The elasticity of iron has been inferred by this method at high pressure (up to 210 GPa).[10,11] The equation of state of cobalt has been measured up to 80 GPa (Ref. 12) and its elastic constants were obtained at zero pressure using traditional ultrasonic methods.[13] In the case of rhenium the equation of state is known up to 215 GPa,[14] its elastic constants and their pressure derivatives have been ultrasonically measured at low pressure.[15] The same experimental method for evaluating lattice strains as in hcp iron has been applied to rhenium in the pressure range 18–37 GPa.[16]

Iron has been studied widely with first-principles theoretical approaches because of its geophysical importance and the well-known failure of the local density approximation (LDA) to the exchange-correlation potential to predict the ferromagnetic bcc ground state.[17] This failure was a major impetus in the development of the generalized gradient approximation (GGA).[18–20] The equation of state of hcp iron under LDA and GGA is well known to high pressures[21–24] and its elastic constants have been calculated by the full-potential linearized muffin-tin orbital method (FP-LMTO),[24] and a total energy tight-binding (TB) method.[5,25] For hcp cobalt calculations have been performed with the LMTO method in the atomic sphere approximation for LDA (Ref. 26) and the linearized combination of atomic orbital method (LCAO) for GGA.[27] There is no previous theoretical work on the elastic constants of hcp cobalt. For rhenium only one study has focused on the hcp phase at high pressure;[28] using FP-LMTO with LDA the equation of state and the elastic constants at zero pressure have been calculated.

We organize the paper as follows. Section II elaborates the computational details of our first-principles calculations and our approach to calculating the elastic constants, the elastic wave velocities, and the acoustic anisotropy. It is followed by a section presenting our results on the magnetic state of the materials studied, their c/a ratios, the equation of state, and the elastic constants as functions of pressure. We compare our results in terms of the elastic wave velocities to high pressure experiments and the Earth's inner core. In Sec. IV we analyze the elastic anisotropy resulting from our calculations, recent experimental and theoretical results, and the predictions from a central nearest-neighbor force model. Finally, we present our conclusions in Sec. V.

II. METHOD

LAPW total energy calculations

We investigate the energetics of hcp iron, cobalt, and rhenium using the full-potential linearized-augmented plane-

wave method (LAPW) (Ref. 29) with both LDA and GGA approximations to the exchange-correlation potential. For LDA the form of Hedin and Lundquist[30] and von Barth and Hedin[31] are used for nonmagnetic and spin-polarized calculations, respectively. For GGA we adopt the efficient formulation of Perdew, Burke, and Ernzhofer.[20]

Core states are treated self-consistently using the full Dirac equation for the spherical part of the potential, while valence states are treated in a semirelativistic approximation neglecting spin-orbit coupling. We investigate ferromagnetic alignment in spin-polarized calculations for all metals and antiferromagnetism for iron. For consistency of the results all parameters in the calculations except for spin-polarization are kept fixed.

For the $3d$ metals $3s$, $3p$, $3d$, $4s$, and $4p$ states are treated as valence electrons for all volumes. For rhenium we treat all electrons up to $4f$ as core, $5d$ and $6s$ as valence states. For rhenium we also have tested other configurations, such as including the $4f$ as valence states, which did not change our results significantly. The muffin-tin radii R_{MT} are 2.0 Bohr for the $3d$ metals, and 2.3 Bohr for rhenium. As spin-orbit coupling of the valence electrons is important for the band structure and other properties of heavy elements, we consider the influence of the spin-orbit term on the equation of state for Re by including it in a variational step.[29]

We carry out total energy calculations over a wide range of volumes for all three metals ($0.7\ V_0$–$1.2\ V_0$, with V_0 the zero pressure volume). At each volume we determine the equilibrium ratio of the lattice constants c/a by performing calculations for several different values of this ratio. The equation of state is obtained by describing the energy-volume curve with a third-order expansion in the Eulerian finite strain.[32]

We have performed convergence tests with respect to Brillouin zone sampling and the size of the basis set, $R_{MT}K_{max}$, where K_{max} is the largest reciprocal space wave vector in the basis set. Converged results are achieved with a $12\times12\times12$ special k-point mesh,[33] yielding 114 k points in the irreducible wedge of the Brillouin zone for the hcp lattice, and up to 468 k points for the monoclinic lattice used in elastic constants calculations. The number of k points in the full Brillouin zone is well above the convergence criterion for elastic constant calculations established by Fast *et al.*[28] The size of the basis set is given by $R_{MT}K_{max}=9.0$, yielding 158 to 311 basis functions, depending on volume. Careful convergence tests show that with these parameters relative energies are converged to better than 0.1 mRy/atom, magnetic moments to better than 0.05 μ_B/atom, and c/a to within 0.025.

Elastic constants

We calculate the elastic constants as the second derivatives of the internal energy with respect to the strain tensor (ε). We choose the applied strains to be isochoric (volume conserving) which has several important consequences: First, we assure the identity of our calculated elastic constants with the stress-strain coefficients, which are appropriate for the calculation of elastic wave velocities; this identity is nontrivial for finite applied pressure.[34,35] Second, the total energy depends on the volume much more strongly than on strain; by choosing volume conserving strains we obviate the separation of these two contributions to the total energy. Third, the change in the basis set associated with the applied strain is minimized, thereby minimizing computational uncertainties.

We obtain the elastic constants at the equilibrium relaxed structure at any volume V by straining the lattice, relaxing the symmetry allowed internal degrees of freedom, and evaluating the total energy changes due to the strain as a function of its magnitude δ.

The bulk modulus K is calculated by differentiating the equation of state. For hexagonal crystals K is the combination of elastic constants

$$K=[C_{33}(C_{11}+C_{12})-2C_{13}^2]/C_S, \tag{1}$$

with

$$C_S=C_{11}+C_{12}+2C_{33}-4C_{13}. \tag{2}$$

The volume dependence of the optimized c/a is related to the difference in the linear compressibilities along the a and c axes (k_a and k_c). The dimensionless quantity R describes this as

$$R=K(k_a-k_c)=-\frac{d\ln(c/a)}{d\ln V}. \tag{3}$$

In terms of the elastic constants,

$$R=(C_{33}-C_{11}-C_{12}+C_{13})/C_S. \tag{4}$$

We calculate C_S by varying the c/a ratio at a given volume, according to the isochoric strain

$$\varepsilon(\delta)=\begin{pmatrix}\delta & 0 & 0\\ 0 & \delta & 0\\ 0 & 0 & (1+\delta)^{-2}-1\end{pmatrix}. \tag{5}$$

The corresponding energy change is

$$E(\delta)=E(0)+C_SV\delta^2+O(\delta^3). \tag{6}$$

In the expressions for C_S, K, and R, C_{11} and C_{12} occur only as a sum. To separate these constants we determine their difference, $C_{11}-C_{12}=2C_{66}$ by applying an orthorhombic strain, space group $Cmcm$. For the strained lattice we use the two atom primitive unit cell, with the atoms in the Wyckoff position $4c$, coordinates $(y,-y,1/4)$. The strain is

$$\varepsilon(\delta)=\begin{pmatrix}\delta & 0 & 0\\ 0 & -\delta & 0\\ 0 & 0 & \delta^2/(1-\delta^2)\end{pmatrix}, \tag{7}$$

leading to a change in total energy:

$$E(\delta)=E(0)+2C_{66}V\delta^2+O(\delta^4). \tag{8}$$

In the unstrained lattice the atomic coordinate is $y=1/3$, but varies under strain.[36] We relax our calculations with respect to this internal degree of freedom.

To determine C_{44} we use a monoclinic strain, space group $C2/m$. The atomic positions in the two atom primitive unit cell are $(1/6,5/6,1/4)$. The strain applied

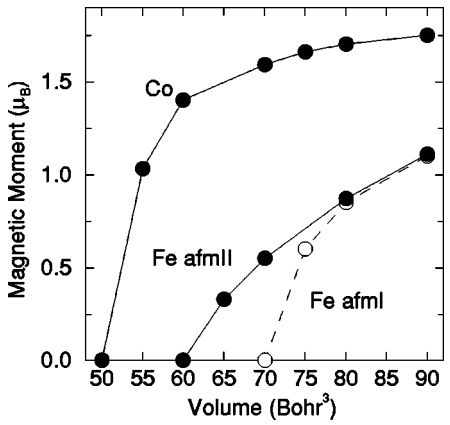

FIG. 1. Magnetic moment per atom within the muffin-tin sphere for the two antiferromagnetic states of iron considered here and the ferromagnetic moment for cobalt as a function of volume.

$$\varepsilon(\delta)=\begin{pmatrix} 0 & 0 & \delta \\ 0 & \delta^2/(1-\delta^2) & 0 \\ \delta & 0 & 0 \end{pmatrix} \tag{9}$$

results in an energy change

$$E(\delta)=E(0)+2C_{44}V\delta^2+O(\delta^4). \tag{10}$$

The equilibrium positions of the atoms are unaffected by this strain and do not need to be redetermined.[36]

While for C_{66} and C_{44} the leading error term is of the order δ^4, for C_S it is of third order in δ. It is therefore crucial to include positive and negative strains in the calculation for C_S. The strain amplitudes applied are typically nine values of δ covering $\pm 4\%$ for C_S; for C_{66} and C_{44}, seven values of δ ranging to 6% are applied. The elastic constants are then given by the quadratic coefficient of polynomial fits to the total energy results; the order of the polynomial fit is determined by a method outlined by Mehl.[37]

From the full elastic constant tensor we can determine the shear modulus μ according to the Voigt-Reuss-Hill scheme[38] and hence the isotropically averaged aggregate velocities for compressional (v_p) and shear waves (v_s)

$$v_p=\sqrt{(K+\tfrac{4}{3}\mu)/\rho}, \quad v_s=\sqrt{\mu/\rho}, \tag{11}$$

with ρ the density.

More generally, the acoustic velocities are related to the elastic constants by the Christoffel equation

$$(C_{ijkl}n_jn_k-M\delta_{il})u_i=0, \tag{12}$$

where C_{ijkl} is the fourth rank tensor description of elastic constants, **n** is the propagation direction, **u** the polarization vector, $M=\rho v^2$ is the modulus of propagation and v the velocity.

The acoustic anisotropy can be described as

$$\Delta_i=\frac{M_i[\mathbf{n}_x]}{M_i[100]}, \tag{13}$$

where $\mathbf{n}_x$ is the extremal propagation direction other than [100] and i is the index for the three types of elastic waves (one longitudinal and the two polarizations of the shear wave). Solving the Cristoffel equation for the hexagonal lattice one can calculate the anisotropy of the compressional (P) wave as

$$\Delta_P=\frac{C_{33}}{C_{11}}. \tag{14}$$

For the shear waves the wave polarized perpendicular to the basal plane ($S1$) and the one polarized in the basal plane ($S2$) have the anisotropies

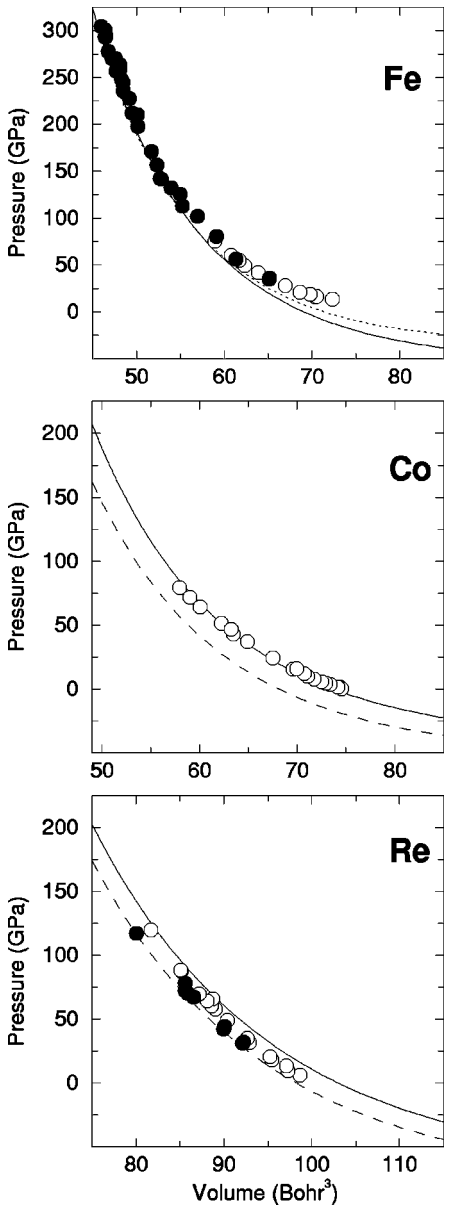

FIG. 2. Equations of state for the hcp metals considered. The upper panel compares the GGA nonmagnetic (solid line) with the afmII structure (dotted line) for iron; Static experimental data is from Ref. 8 (open circles) and Ref. 9 (filled circles). The lower two figures show the equations of state for ferromagnetic cobalt and nonmagnetic rhenium, GGA results are shown in solid, LDA in dashed curves. The static experimental data for cobalt are from Ref. 12, for rhenium static (open circles) and reduced shock wave data (filled circles) are from Ref. 7 and Ref. 48, respectively.

TABLE I. Equation-of-state parameters from a third-order finite Eulerian strain expansion of the energy-volume relation for the hcp transition metals. V_0, K_0 are the zero pressure volume and bulk modulus, respectively; K_0' the pressure derivative of the bulk modulus. For experimental values the bulk modulus is calculated from the elastic constants at ambient pressure.

		E_0 (Ry/atom)	V_0 (Bohr^3)	K_0 (GPa)	K_0'
Fe	expt (Ref. 9)		75.4	165	5.3
	LDA nm	−2541.1046	64.7	344	4.4
	GGA nm	−2545.6188	69.0	292	4.4
	GGA afmI	−2545.6195	70.5	210	5.5
	GGA afmII	−2545.6212	71.2	209	5.2
	LMTO GGA (Ref. 24)		65.5	340	
Co	expt (Ref. 13)		74.9	190	3.6(2)
	LDA fm	−2782.1081	68.0	255	4.0
	GGA fm	−2786.7364	73.6	212	4.2
	LCAO GGA (Ref. 27)		76.2	214	
	LMTO LDA (Ref. 26)	−2782.173	71.1	276	
Re	expt (Ref. 49 and 13)		99.3	365	
	LDA nm	−33416.1921	98.2	382	3.9
	GGA nm	−33436.2502	103.0	344	3.9
	LMTO LDA (Ref. 28)		98.8	447	

$$\Delta_{S1}=\frac{C_{11}+C_{33}-2C_{13}}{4C_{44}}, \quad \Delta_{S2}=\frac{C_{44}}{C_{66}}. \tag{15}$$

While for $S2$ and P waves the extremum occurs along the c axis, for $S1$ it is at an angle of 45° from the c axis in the a-c plane. We note that an additional extremum may occur for the compressional wave propagation at intermediate directions depending on the values of the elastic constants.

III. RESULTS

Magnetism

We find a stable ferromagnetic state only in cobalt. It is stabilized over a wide volume range with the magnitude of the moment decreasing with pressure in agreement with previous theoretical results on the pressure dependence of magnetic moments[23] in other transition metals. Only at the smallest volume considered (50 Bohr^3, 180 GPa) is the moment vanishingly small (Fig. 1). LDA and GGA yield consistent results and predict a zero pressure magnetic moment of 1.55 μ_B, in excellent agreement with experiment (1.58 μ_B).[39]

In the case of hcp iron, we also investigate two antiferromagnetic states. The first consists of atomic layers of opposing spin perpendicular to the c axis (afmI). The other arranges the planes of opposite spins normal to the [100] direction in the hcp lattice; this can be described by the orthorhombic representation of the hcp unit cell (space group $Pmma$) with spin up in the (1/4,0,1/3) and spin down in the (1/4,1/2,5/6) position (afmII). We find that both structures are more stable than the non-spin-polarized state and that afmII is energetically favored over afmI. For both antiferromagnetic states the moment is strongly pressure dependent. For afmI it vanishes at volumes larger than V_0 (Fig. 1), in excellent agreement with results of Asada and Terakura.[22] The other structure, afmII, possesses a magnetic moment well into the stable pressure regime of hcp iron, up to ~40 GPa (Fig. 1). Because of frustration on the triangular lattice, it is possible that more complex spin arrangements such as incommensurate spin waves as for fcc iron[40] or a spin glass are still more energetically favorable than afmII.

Diamond anvil cell *in situ* Mössbauer measurements of hcp iron[41] have shown no evidence of magnetism in the hcp phase. The low antiferromagnetic moment we calculate in the stable hcp regime and the significant hysteresis of the bcc-hcp transition[41] might explain that no magnetism in hcp iron has been detected in the high pressure Mössbauer experiment. In this context it may be relevant that indirect evidence for magnetism exists at low pressure. Epitaxially grown iron-ruthenium superlattices have shown magnetism occurring in hcp iron multilayers.[42] Its character, however, is still controversial.[43,44]

c/a ratios

For all materials studied the c/a ratio agrees with experimental data to within 2% and is essentially independent of the exchange correlation potential (GGA or LDA). Equilibrium c/a ratios for iron range from 1.58 at zero pressure to 1.595 at 320 GPa. This is consistent with experimental measurements[8,9] in the range of 15–300 GPa, which have shown considerable scatter. For cobalt the zero pressure c/a ratio is calculated as 1.615, increasing to 1.62 at a pressure of almost 200 GPa. The zero pressure c/a is slightly lower than the experimental value of 1.623.[39] Diamond anvil cell experiments have found a higher value of c/a, as much as the ideal value (1.633),[12] this discrepancy might be due to the coexistence of hcp and metastable fcc cobalt in the polycrystalline sample.[12] The c/a ratio for rhenium (1.615) does not

change over the whole pressure range studied—and is in good agreement with experimental results (1.613).[14]

Equation of state

For the equation of state of rhenium, LDA shows better agreement with experimental data than does GGA (Fig. 2, Table I). GGA overestimates the zero pressure volume and softens the bulk modulus, supporting a general pattern seen in prior density functional calculations using GGA for other $5d$ metals.[45,46] Including spin-orbit coupling in the calculation has little effect on the equation of state parameters, resulting in less than 1% change in the zero pressure volume and 2% in the bulk modulus. For cobalt, as for other $3d$ metals GGA is superior to LDA and reproduces the experimental equation-of-state to within 2% in volume and 10% in bulk modulus (Fig. 2, Table I).

The discrepancy in the equation-of-state parameters of hcp iron between non-spin-polarized calculations and experiment is significantly larger than for the other two metals studied here (Table I) or other transition metals.[45,46] The zero pressure volume is underestimated by $\sim 9\%$, and the zero pressure bulk modulus is too stiff by 75% (Table I). Especially at low pressure the nonmagnetic equation of state deviates considerably from experimental values, while at high pressure the agreement is very good (Fig. 2). The stabilization of antiferromagnetic states at low pressure can account for some of the discrepancy. For afmII magnetism persists to volumes smaller than V_0, resulting in a larger zero pressure volume, reducing the difference with experiment to 5%, and lowering the bulk modulus considerably (Table I). This is still larger than the difference in V_0 for cobalt and for cubic iron phases ($<3\%$).[23,24] We attribute the remaining discrepancy between low pressure experimental data and the afmII equation of state (Fig. 2) to the approximations in GGA and the possible stabilization of more complex spin arrangements than those considered here.

Elasticity

The agreement of the calculated elastic constants for cobalt and rhenium with zero pressure experimental results[13,15] is excellent with a root mean square error of better than 20 GPa for both metals and both exchange-correlation potentials (Fig. 3, Tables II and III). The initial pressure derivative of the elastic constants for rhenium is also well reproduced by the calculations (Fig. 3). LDA and GGA exchange-correlation potentials give almost equally good agreement, the minor differences arising primarily from differences in the bulk modulus (Tables I, II, and III).

Our elastic constant calculations for rhenium and iron do not agree with the results of lattice strain experiments (Fig. 3, Tables III and IV). For rhenium the overall agreement between these experiments and our elastic constants is better than for iron. C_{11} and C_{12} agree well over the pressure range of the experiments, while the other longitudinal (C_{33}) and off-diagonal constant (C_{13}) differ significantly (Fig. 3, Table III)). The shear elastic modulus (C_{44}) shows the largest discrepancy of all elastic constants (factor of 1.5). For iron the results of the lattice strain experiments and our calculations are in reasonable agreement for the off-diagonal constants only. The longitudinal moduli we obtain at 60 Bohr^3 and 50 Bohr^3 (~ 50 GPa and ~ 200 GPa, respectively) are larger by approximately 50%. This is partly related to the overestimated bulk modulus in the calculations. The largest discrepancy, as in the case of rhenium, occurs in the shear elastic constants (C_{44} and C_{66}).

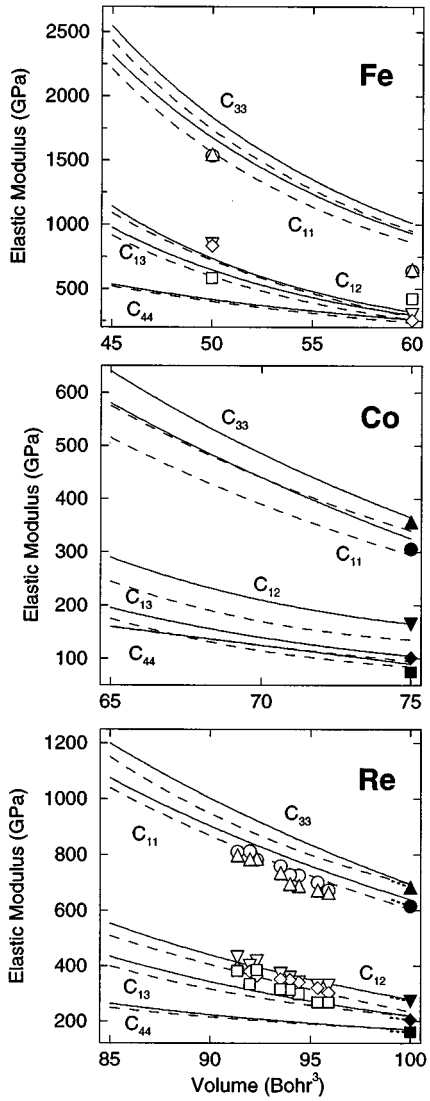

FIG. 3. The elastic constants of hcp iron from our calculations are shown in the upper figure. The lines are Eulerian finite strain fits to the theoretical results at 45, 50, and 60 Bohr^3: solid (GGA), dashed (LDA). Lattice strain experiments from Refs. 10 and 11 are shown by the open symbols: C_{11} (○), C_{33} (△), C_{12} (▽), C_{13} (◇), and C_{44} (□). In the middle panel elastic constants for hcp cobalt are shown as a function of volume. The curve is again a fit to the calculations at 65, 70, and 75 Bohr^3. GGA is shown in solid, LDA in dashed lines. At the zero pressure volume they are compared to ultrasonic experiments from Ref. 13 (filled symbols as above). The lower figure shows the equivalent for rhenium with calculations at 85, 93, and 100 Bohr^3. The thick dotted lines indicate the initial pressure derivatives as determined from ultrasonic measurements (Ref. 15). For lattice strain experiments from Ref. 16 open symbols are used again.

Aggregate properties such as the bulk and shear modulus, and the compressional and shear wave velocity are in some-

TABLE II. Elastic constants of hcp cobalt from theory (GGA, LDA) and experiment. $C_{66}=\frac{1}{2}(C_{11}-C_{12})$ is added for comparison with C_{44}.

Volume (Bohr^3)	C_{11} (GPa)	C_{33} (GPa)	C_{12} (GPa)	C_{13} (GPa)	C_{44} (GPa)	C_{66} (GPa)
			Ultrasonic Experiment (0 GPa) (Ref. 13)			
74.9	306	357	165	102	75	71
			GGA			
75.0	325	365	165	105	90	80
70.0	440	485	210	140	125	115
65.0	580	640	290	195	160	145
			LDA			
75.0	295	340	135	85	95	80
70.0	390	440	170	115	125	110
65.0	515	575	245	175	160	135

what better agreement between the theoretical results and the lattice strain experiment for both rhenium and iron (Figs. 4 and 5). For rhenium, theory and experiment differ by less than 15% in bulk and shear modulus (Fig. 4). For iron the discrepancy is considerable at intermediate pressure but becomes smaller with increasing pressure, as already seen for the equation of state (Figs. 2 and 5). At $\sim$200 GPa the difference in bulk modulus between GGA and experiment is less than 5% and the elastic wave velocities differ by $\sim$10%. The shear modulus differs by 25% even at high pressure.

For iron the comparison with previous theoretical results gives a more coherent picture. While the longitudinal elastic constants from our calculations are larger by 10–20 % compared to TB (Ref. 25) and FP-LMTO results[24] (Table IV), the elastic anisotropy is similar: the pairs of longitudinal, shear, and off-diagonal elastic moduli display similar values. For the TB study this is true over the whole pressure range considered, for the FP-LMTO calculations only at low pressure; the ratio of the off-diagonal constants (C_{12}/C_{13}) is strongly pressure dependent in that study, varying from 0.9 at zero pressure to 0.6 at 400 GPa.

IV. DISCUSSION

We find that the elastic anisotropy [Eqs. (14) and (15)] is similar for all three metals studied here. The magnitude of the anisotropy is $10\pm2\%$ for the longitudinal anisotropy and Δ_{S1}, and $30\pm3\%$ for Δ_{S2} and is nearly independent of pressure (Fig. 6). This is consistent with the experimentally observed behavior of other hcp transition metals, all of which—except for the filled *d*-shell metals zinc and cadmium—show anisotropy of similar magnitude (Fig. 6).

These results can be understood by comparison to a hcp crystal interacting with central nearest-neighbor forces (CNNF).[47] For this model the elastic anisotropy is independent of the interatomic potential to lowest order in P/C_{11}, hence the anisotropy is dependent on the symmetry of the crystal only. Born and Huang[47] have shown that from this CNNF model the elastic constants scale as 32:29:11:8:8 for $C_{33}:C_{11}:C_{12}:C_{13}:C_{44}$, yielding $\Delta_P=32/29$, $\Delta_{S1}=8/9$, and $\Delta_{S2}=45/32$ (Fig. 6).

The experimentally determined elastic anisotropies of rhenium and hcp iron at high pressure from lattice-strain mea-

TABLE III. Elastic constants of hcp rhenium from theory (present work: GGA, LDA) and experiment. $C_{66}=\frac{1}{2}(C_{11}-C_{12})$ is added for comparison with C_{44}.

Volume (Bohr^3)	C_{11} (GPa)	C_{33} (GPa)	C_{12} (GPa)	C_{13} (GPa)	C_{44} (GPa)	C_{66} (GPa)
			Ultrasonic Experiment (0 GPa) (Ref. 15)			
99.3	616	683	273	206	161	172
			Lattice Strain Experiment (26.5 GPa) (Ref. 16)			
93.5	760(65)	735(165)	370(40)	355(50)	320(60)	195(60)
			GGA			
100.0	640	695	280	220	170	180
93.0	815	900	385	300	205	215
85.0	1075	1200	555	435	265	260
			LDA			
100.0	605	650	235	195	175	185
93.0	780	855	350	280	200	215
85.0	1040	1150	510	400	250	265
			FP-LMTO LDA (Ref. 28)			
98.7	837	895	293	217	223	272

TABLE IV. Elastic constants for nonmagnetic hcp Fe under compression (present work: GGA, LDA); the pressure range covered corresponds to approximately 50 GPa to 350 GPa, almost the pressure in the Earth's center. For comparison results of other studies at ~60 Bohr^3 are included. $C_{66}=\frac{1}{2}(C_{11}-C_{12})$ is added for comparison with C_{44}.

Volume (Bohr^3)	C_{11} (GPa)	C_{33} (GPa)	C_{12} (GPa)	C_{13} (GPa)	C_{44} (GPa)	C_{66} (GPa)
			Lattice Strain Experiment (50 GPa) (Ref. 10)			
60	640(55)	650(85)	300(55)	255(40)	420(25)	170(55)
			GGA			
60	930	1010	320	295	260	305
50	1675	1835	735	645	415	475
45	2320	2545	1140	975	400	590
			LDA			
60	860	950	280	260	235	290
50	1560	1740	720	595	415	420
45	2210	2435	1090	915	535	560
			Tight-Binding (Ref. 25)			
60	845	900	350	340	235	245
			FP-LMTO GGA (Ref. 24)			
60	870	810	255	320	235	310

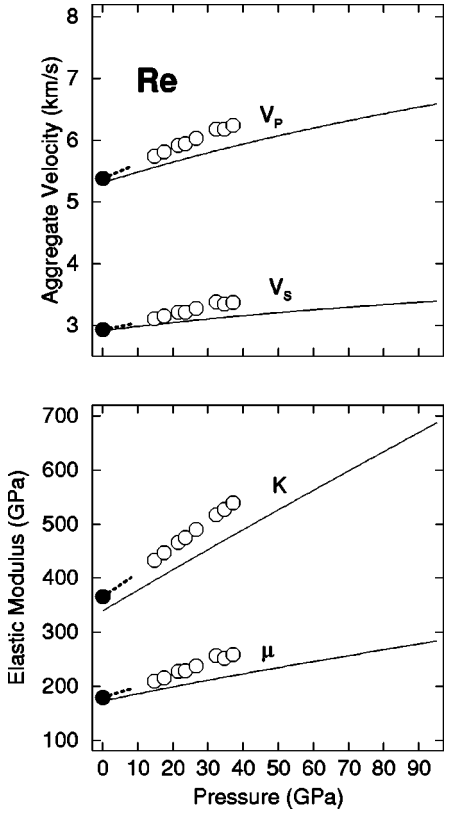

FIG. 4. Isotropic properties for hcp rhenium in comparison to experiments. The lower panel shows the bulk (K) and shear modulus (μ) of our calculations (GGA) in solid lines. The ultrasonic experiments at ambient condition from Ref. 15 are shown in filled circles with the initial pressure dependence in thick dotted lines. Lattice strain experiments from Ref. 16 are shown in open symbols. The upper panel uses the same symbols as the lower one for the compressional (v_p) and shear wave velocity (v_s).

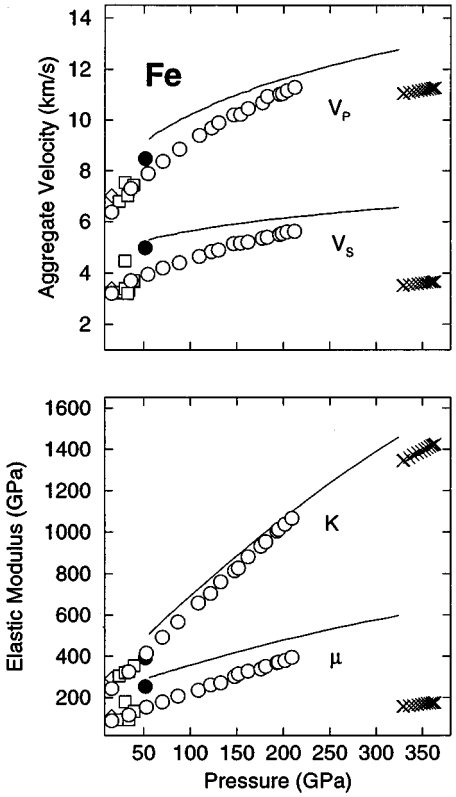

FIG. 5. Bulk properties for hcp iron in comparison to experiments and Earth's inner core. The lower panel shows the bulk (K) and shear modulus (μ) of our calculations (GGA) in solid lines. Diamond anvil cell experimental results are from Refs. 10 (●) and 11 (○ and □, denoting two different approaches). Ultrasonic measurements in a multianvil experiment (◇) are from Ref. 11 as well. The crosses display seismic observations of the inner core. The lower figure uses the same symbols as the upper one for the compressional (v_p) and shear wave velocity (v_s).

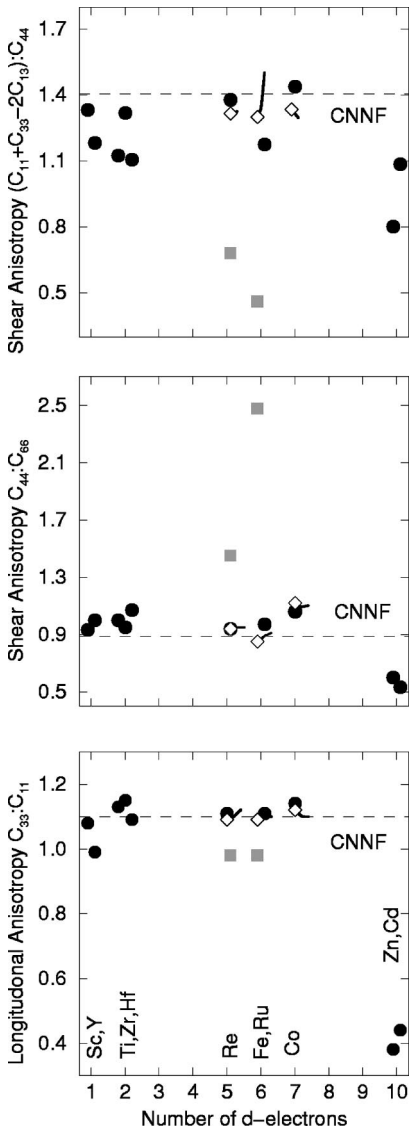

FIG. 6. As a measure of anisotropy the elastic constant ratios C_{11}/C_{33}, $(C_{11}+C_{33}-2C_{13})/4C_{44}$, and C_{44}/C_{66}, which govern the compressional (Δ_P) and shear wave anisotropy (Δ_{S1} and Δ_{S2}, respectively) of the single crystal, are shown as a function of the number of *d* electrons. The upper figure shows the shear elastic anisotropy Δ_{S1}, the middle Δ_{S2}, and the lower the ratio of the longitudinal elastic constants Δ_P. For all transition metals crystallizing in the hcp phase filled circles are used. The dashed lines show the CNNF model predictions. High pressure lattice strain results for iron from Ref. 10 and for rhenium from Ref. 16 are displayed with gray squares. Our results are the open diamonds with the pressure dependence shown in solid lines connected to the symbols.

surements differ substantially from our theoretical predictions, previous theoretical calculations, the behavior of all other hcp transition metals, and the simple CNNF model (Fig. 6). The shear anisotropy in particular is very different in the high pressure experiments as compared with all other relevant results. We suggest that this discrepancy may arise from assumptions made in the data analysis. In particular, the assumption that the state of stress on all crystallographic planes is identical.[10] This condition may not be satisfied in a material undergoing anisotropic deformation (e.g., dominated by basal slip), behavior that is observed for many hcp transition metals.

Theory shows much better agreement with lattice-strain experiments in terms of the isotropically averaged moduli. Even so, the agreement in the case of rhenium is much better than for iron.

V. CONCLUSIONS

The equations of state and the elastic constant tensor at zero pressure and under compression for two ambient condition hcp transition metals, cobalt and rhenium, and for the high pressure phase of iron, hcp, are calculated by means of the first-principles LAPW method. We find a ferromagnetic ground state for cobalt and an antiferromagnetic one for iron, with the antiferromagnetic moment vanishing at 60 Bohr[3]. The equations of state for the metals are in good agreement with experiment, as are the elastic constants and pressure derivatives of the elastic constants for cobalt and rhenium at ambient pressure.

Elastic constants for iron under high pressure as inferred from lattice-strain experiments differ significantly from our theoretical results. Similarly large discrepancies are also found between theory and high pressure static experiments on rhenium. The lattice-strain experiments also lead to large values of the shear anisotropy that differ from that of all other open shell hcp transition metals. Given the excellent agreement of the theoretical elastic constants for cobalt and rhenium with experiment at zero pressure, we suggest that a re-examination of the lattice-strain experiments for rhenium and iron is warranted.

ACKNOWLEDGMENTS

We greatly appreciate helpful discussions with Tom Duffy, Rus Hemley, Dave Mao, and Per Söderlind. The work was supported by the National Science Foundation under Grant No. EAR-9614790, and by the Academic Strategic Alliances Program of the Accelerated Strategic Computing Initiative (ASCI/ASAP) under subcontract No. B341492 of DOE Contract No. W-7405-ENG-48 (REC). Computations were performed on the SGI Origin 2000 at the Department of Geological Sciences at the University of Michigan and the Cray J90/16-4069 at the Geophysical Laboratory, support by NSF Grant No. EAR-9304624 and the Keck Foundation.

[1] I. Jackson, S. K. Revcolevschi, and J. Berthon, J. Geophys. Res. **95**, 21 671 (1990).

[2] H. Shimizu, M. Ohnishi, S. Sasaki, and Y. Ishibashi, Phys. Rev. Lett. **74**, 2820 (1995).

[3] K. C. Creager, Nature (London) **356**, 309 (1992).

[4] J. Tromp, Nature (London) **366**, 678 (1993).

[5] L. Stixrude and R. E. Cohen, Science **267**, 1972 (1995).

[6] X. Song and P. G. Richards, Nature (London) **382**, 221 (1996).

[7] R. Jeanloz, B. K. Godwal, and C. Meade, Nature (London) **349**, 687 (1991).
[8] A. P. Jephcoat, H. K. Mao, and P. M. Bell, J. Geophys. Res. **91**, 4677 (1986).
[9] H. K. Mao, Y. Wu, L. C. Chen, J. F. Shu, and A. P. Jephcoat, J. Geophys. Res. **95**, 21 737 (1990).
[10] A. K. Singh, H. K. Mao, J. Shu, and R. J. Hemley, Phys. Rev. Lett. **80**, 2157 (1998).
[11] H. K. Mao, J. Shu, G. Shen, R. J. Hemley, B. Li, and A. K. Singh, Nature (London) **396**, 741 (1998); (erratum) (to be published).
[12] H. Fujihisa and K. Takemura, Phys. Rev. B **54**, 5 (1996).
[13] H. R. Schober and H. Dederichs, in *Elastic Piezoelectric Pyroelectric Piezooptic Electrooptic Constants and Nonlinear Dielectric Susceptibilities of Crystals*, edited by K.-H. Hellwege and A. W. Hellwege, Landolt Börnstedt, New Series III, Vol. 11a (Springer, Berlin, 1979).
[14] Y. K. Vohra, S. J. Duclos, and A. L. Ruoff, Phys. Rev. B **36**, 9790 (1987).
[15] M. H. Manghnani, K. Katahara, and E. S. Fisher, Phys. Rev. B **9**, 1421 (1974).
[16] T. S. Duffy *et al.*, in *High Pressure Materials Research*, edited by R. M. Wentzcovitch, R. J. Hemley, W. J. Nellis, and P. Y. Yu, MRS Symposia Proceedings No. 499 (Materials Research Society, Pittsburgh, 1998), p. 145.
[17] C. S. Wang, B. M. Klein, and H. Krakauer, Phys. Rev. Lett. **54**, 1852 (1985).
[18] J. P. Perdew and Y. Wang, Phys. Rev. B **33**, 8800 (1986).
[19] J. P. Perdew, J. A. Chevary, S. H. Vosko, K. A. Jackson, D. J. Singh, and C. Fiolhais, Phys. Rev. B **46**, 6671 (1992).
[20] J. Perdew, K. Burke, and M. Ernzhofer, Phys. Rev. Lett. **77**, 3865 (1996).
[21] P. Bagno, O. Jepsen, and O. Gunnarsson, Phys. Rev. B **40**, 1997 (1989).
[22] T. Asada and K. Terakura, Phys. Rev. B **46**, 13 599 (1992).
[23] L. Stixrude, R. E. Cohen, and D. J. Singh, Phys. Rev. B **50**, 6442 (1994).
[24] P. Söderlind, J. A. Moriarty, and J. M. Wills, Phys. Rev. B **53**, 14 063 (1996).
[25] R. E. Cohen, L. Stixrude, and E. Wasserman, Phys. Rev. B **56**, 8575 (1997).
[26] B. I. Min, T. Oguchi, and A. J. Freeman, Phys. Rev. B **33**, 7852 (1986).
[27] T. C. Leung, C. T. Chan, and B. N. Harmon, Phys. Rev. B **44**, 2923 (1991).
[28] L. Fast, J. M. Wills, B. Johansson, and O. Eriksson, Phys. Rev. B **51**, 17 431 (1995).
[29] D. J. Singh, *Planewaves, Pseudopotentials and the LAPW Method* (Kluwer, Norwell, 1994).
[30] L. Hedin and B. I. Lundquist, J. Phys. C **4**, 2064 (1971).
[31] U. von Barth and L. Hedin, J. Phys. C **5**, 1629 (1972).
[32] F. Birch, J. Geophys. Res. **95**, 227 (1952).
[33] H. J. Monkhorst and J. D. Park, Phys. Rev. B **13**, 5188 (1976).
[34] D. J. Wallace, *Thermodynamics of Crystals* (Wiley, New York, 1972).
[35] T. H. K. Barron and M. L. Klein, Proc. Phys. Soc. London **85**, 523 (1965).
[36] M. Nastar and F. Willaime, Phys. Rev. B **51**, 6896 (1995).
[37] M. J. Mehl, Phys. Rev. B **47**, 2493 (1993).
[38] R. Hill, J. Mech. Phys. Solids **11**, 357 (1963).
[39] H. P. Meyer and W. Sucksmith, Proc. R. Soc. London, Ser. A **207**, 427 (1951).
[40] M. Uhl and J. Kübler, J. Phys.: Condens. Matter **9**, 7885 (1997).
[41] R. D. Taylor, M. P. Pasternak, and R. Jeanloz, J. Appl. Phys. **69**, 6126 (1991).
[42] M. Maurer *et al.*, J. Magn. Magn. Mater. **93**, 15 (1991).
[43] M. C. Saint-Lager, D. Raoux, M. Brunel, M. Piecuch, M. Elkaim, and J. P. Lauriat, Phys. Rev. B **51**, 2446 (1995).
[44] D. Knab and C. Koenig, J. Magn. Magn. Mater. **93**, 398 (1991).
[45] B. Barbiellini, E. G. Moroni, and T. Jarlborg, J. Phys.: Condens. Matter **2**, 7597 (1990).
[46] M. Körling and J. Häglund, Phys. Rev. B **45**, 13 293 (1992).
[47] M. Born and K. Huang, *Dynamical Theory of Crystal Lattices* (Clarendon, Oxford, 1954).
[48] S. P. Marsh, *LASL Shock Hugoniot Data* (University of California Press, Berkeley, 1980).
[49] C. Kittel, *Introduction to Solid State Physics* (Wiley, New York, 1976).